PHYSICAL REVIEW C **95**, 064602 (2017)

Measurement of the cross section of the residues from the ^{11}B-induced reaction on ^{89}Y and ^{93}Nb: Production of ^{97}Ru and ^{101m}Rh

Deepak Kumar and Moumita Maiti*
Department of Physics, Indian Institute of Technology Roorkee, Roorkee-247667, Uttarakhand, India
(Received 6 February 2017; revised manuscript received 24 March 2017; published 2 June 2017)

Background: The heavy-ion induced reactions on intermediate mass targets are complex in nature, even at the low energies. To understand those nuclear reaction phenomena in detail, more experimental studies are required in a wide range of energies.

Purpose: Investigation of heavy-ion reactions by measuring production cross sections of the residues produced in the ^{11}B-induced reactions on ^{89}Y and ^{93}Nb at low energies, near and above the barrier, and to check the effectiveness of the different nuclear models to explain them. Further, aim is also to optimize the production parameters of neutron deficient medically relevant ^{97}Ru and ^{101m}Rh radioisotopes produced in those reactions, respectively.

Method: The ^{11}B beam was allowed to impinge on ^{89}Y and ^{93}Nb foils supported by an aluminum (Al) catcher foil, arranged in a stack, in 27.5–58.7 and 30.6–62.3 MeV energy range, respectively. The off-line γ-ray spectrometry was carried out after the end of bombardment to measure the activity of the radionuclides produced in each foil and cross sections were calculated. Measured cross-sectional data were analyzed in terms of compound and precompound model calculations.

Results: The measured cross sections of ^{97,95}Ru, ^{96,95,94}Tc, ^{93m}Mo, ^{90m}Y radionuclides produced in the ^{11}B+^{89}Y reaction, and ^{101,100,99}Pd, ^{101m,100,99m}Rh, ^{97}Ru produced in the ^{11}B+^{93}Nb reaction showed good agreement with the model calculations based on the Hauser-Feshbach formulation and exciton model. Unlike theoretical estimation, consistent production of ^{90m}Y was observed in the ^{11}B+^{89}Y reaction. Substantial pre-equilibrium contribution was noticed in the 3n reaction channel in both reactions.

Conclusions: Theoretical estimations confirmed that major production yields are mostly contributed by the compound reaction process. Pre-equilibrium emissions contributed at the high energy tail of the 3n channel for both reactions. Moreover, an indirect signature of a direct reaction influence was also observed in the ^{90m}Y production.

DOI: 10.1103/PhysRevC.95.064602

I. INTRODUCTION

The comprehensive study on fusion reactions of tightly and weakly bound stable heavy projectiles with medium and heavy targets has been performed and discussed in the literature for many decades [1,2]. However, the strength of reaction processes, such as complete-incomplete fusion, deep inelastic scattering, quasifission, precompound processes near the Coulomb barrier, nucleon transfer reactions, etc., observed in the low-energy heavy ion induced reactions has not yet been understood in a full-fledged fashion [3–10]. In spite of that, its importance to understand the synthesis of superheavy elements [11,12], nucleosynthesis process necessary for the star evolution[13], quantum mechanical tunneling phenomenon near sub-barrier energies, fusion hindrance phenomenon at deep sub-barrier energies [14,15], behavior of nuclei far from the stability region investigated using radioactive ion beam on the medium/heavy mass targets [16–18], etc., fascinate researchers and made it a central topic for nuclear physics research in recent years.

In view of this quest, a systematic study of boron (^{11}B) induced reaction on intermediate mass targets: yttrium (^{89}Y) and niobium (^{93}Nb), has been reported in the ~2.5–5.5 MeV/nucleon energy range. Production of ^{97,95}Ru, ^{96,95,94}Tc, ^{93m}Mo, ^{90m}Y and ^{101,100,99}Pd, ^{101m,100,99m}Rh, ^{97}Ru radionuclides are observed at ^{89}Y and ^{93}Nb targets, respectively. This article contributes to the study of the nuclear reaction mechanisms involved in the production of various radioisotopes. It is also important to examine the reaction cross section predictive capability of recent upgrades in modern reaction codes for model calculations. Optimization of the production of neutron deficient medically relevant radionuclides, ^{97}Ru and ^{101m}Rh, which are produced in ^{11}B+^{89}Y and ^{11}B+^{93}Nb reactions, respectively, has also been discussed.

The ^{97}Ru radionuclide could be used in both diagnostic and therapeutic processes due to its suitable half-life (2.83 d), low-lying intense γ-rays: 215.70 keV (85.62%) and 324.49 keV (10.79%) energy, and high chemical reactivity. It could be produced in the no-carrier-added (NCA) state, which is the prerequisite of clinical applications [19], from ^{11}B+^{89}Y reaction. Initially, ^{97}Ru was produced mainly by the bombarding high energy proton beams on different targets: rhodium (^{103}Rh), technetium (^{99}Tc), [20–22]. Besides, α-particle or ^{3}He induced reactions on natural molybdenum targets were also led to the production of ^{97}Ru [23–25]. Recently, heavy ion (^{7}Li, ^{11}B, ^{12}C) induced reactions on natural Nb and Y metals were also studied by our group to produce NCA ^{97}Ru [26–30].

On the other hand, low-lying high intense γ-rays of ^{101m}Rh help in the *in vivo* monitoring by using a scintillation camera,

*moumifph@iitr.ac.in, moumifph@gmail.com

while emission of Auger, Coster-Kronig electrons, and x-rays aid in therapeutic applications. The ^{101m}Rh (4.34 d) decays mainly by electron capture (92.8 %) to stable ^{101}Ru by emitting 306.9 keV (81 %) and 545.1 keV (4.3 %) γ-rays and by isomeric transition (IT) (7.2 %) to ^{101}Rh (3.3 a), which finally decays to ^{101}Ru.

So far, production of ^{101m}Rh has been studied using light ion ($p,d,{}^{3}$He, ^{4}He) induced reactions only. ^{101m}Rh was produced through the decay of its precursors ^{101}Pd and ^{101}Ag, which were populated in p-induced reactions on the ^{103}Rh, $^{\rm nat}$Pd, and $^{\rm nat}$Ag targets [31–37]. In the deuteron-induced reactions, the production of ^{101m}Rh using a ^{103}Rh target was measured by Hermanne *et al.*, Detrói *et al.* in different energy regions [38–40]. Direct and cumulative production of ^{101m}Rh in the $d+{}^{\rm nat}$Pd reaction was also experimented by Detrói *et al.* [41], however the production was significantly low. Apart from these, production of ^{101m}Rh isomer was reported by Skakun *et al.* [42] for the ^{3}He-induced reaction via ^{101}Ru(^{3}He,x)^{101m}Rh (cum) and ^{102}Ru(^{3}He,x)^{101m}Rh reactions.

Thus we have gone through the current interest to study the heavy ion induced reactions and the production of ^{97}Ru and ^{101m}Rh radionuclides in those reactions. The experimental procedure and brief review of the nuclear model calculations are described in Secs. II and III, respectively. Section IV discusses the results and Sec. V finally concludes the report.

II. EXPERIMENT

The experiment was performed at the BARC-TIFR Pelletron facility, Mumbai, India. Stacked foil activation technique was used to explore ^{89}Y+^{11}B and ^{93}Nb+^{11}B reactions. A stack of targets was prepared by placing 2–3 target foils each one of which was backed by an aluminum (Al) catcher foil so that target and backing appear in an alternative fashion. A typical experimental setup to irradiate the stack foil arrangement is shown in Fig. 1. Each target stack was bombarded by the ^{11}B^{5+} beam for a stipulated time. Beam current was kept almost constant during the experiment. The total charge passed through the target was measured by an electron suppressed Faraday cup placed at the back of the target assembly during the beam-on period. The time of irradiation was decided by the projectile flux and the half-lives of the product radioisotopes. A total of 4–5 such stacks was irradiated

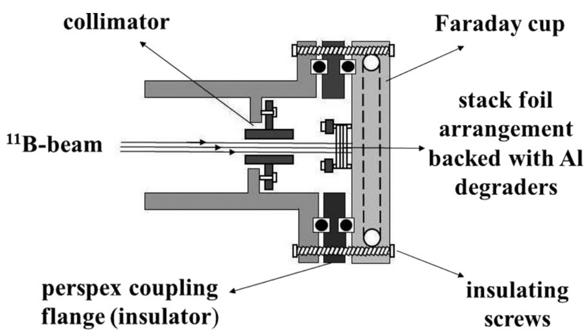

FIG. 1. A schematic diagram of a typical stack foil activation setup.

individually for each target-projectile combination varying the incident energy of ^{11}B with a slight overlap between them.

Spectroscopically pure (99.99%) natural yttrium and niobium foils were procured from the Alfa Aesar. Self-supporting thin foils of those metals were made by uniform rolling in a machine. Thicknesses of the thin Y and Nb foils were between 0.84–2.9 mg/cm^2 and 1.2–2.1 mg/cm^2, respectively. The Al-backing foils had thickness between 1.5–2 mg/cm^2. Annular aluminum holders with an inner and outer diameter 12 and 20 mm, respectively, were used to mount the foils. The large area of the Al foil ensures the complete collection of the recoiled residues, if recoiled any, in the beam direction. The Al foils also served the purpose of an energy damper so that suitable energy separation between consecutive target foils could be achieved. Energy degradation of the projectile in each foil was estimated by the stopping and range of ions in matter (SRIM) code [43]. The ^{11}B energy at a target is typically the average of the incident and outgoing beam energy.

After the end of bombardment (EOB), the residual radionuclides produced in each target foil (Y and Nb) were identified and quantified with the help of γ-ray spectrometry using a broad energy germanium (BEGe) based detector attached with a PC operating with the GENIE-2K software. The detector was calibrated by using standard sources, ^{152}Eu (13.506 a), ^{137}Cs (30.08 a), ^{60}Co (5.27 a), ^{133}Ba (10.51 a), of known activity. The energy resolution of the detector was $\leqslant$2.0 keV at 1332 keV energy.

The activity of the residuals was measured in a fixed geometry over a longer period of time in the regular intervals to follow their decay profile. The activity of the residuals at the EOB was measured from the background-subtracted peak area count rate (counts/sec). Production cross section of the residues at each incident energy was calculated from the activation formula. The detail description of the activity and cross-section measurement is available in our previous reports [26,44,45]. Nuclear spectroscopic data of the residual radionuclides are listed in Table I [46].

The error introduced in the cross section measurement was mainly due to the nonuniformity of samples and in measuring its thickness (~5%), fluctuation of beam current (~5%), efficiency calibration of the detector (~2%). Some other sources such as the branching intensity of characteristic γ-rays, counting statistics, beam energy degradation while traversing through the successive target foils (straggling effects), etc., are also responsible; however, these were negligible in this case [47,48]. The total uncertainty associated with the cross section measurement was determined considering all those factors and the data was presented in this article up to 95% confidence level.

III. ANALYSIS OF MEASURED DATA

1. PACE4

Compound reaction contribution in the produced residues at different bombarding energies in the ^{11}B+^{89}Y and ^{11}B+^{93}Nb reactions was extracted with the help of a statistical model code PACE4 [49], built on the Hauser-Feshbach (HF) formulation where angular momentum coupling is considered in each

TABLE I. Spectroscopic decay data [46] for the observed radioisotopes and list of contributing process in the $^{11}B + ^{89}Y$ and $^{11}B + ^{93}Nb$ reactions.

Nuclides(J^π)	Half-life	decay mode(%)	E_γ(keV)	I_γ(%)	Contributing reactions	E_{th}[a] (MeV)
^{97}Ru(5/2$^+$)	2.83 d	ϵ(100)	215.70	85.62	^{89}Y(^{11}B, 3n)	19.26
			324.49	10.79		
^{95}Ru(5/2$^+$)	1.64 h	ϵ(100)	336.40	70.20	^{89}Y(^{11}B, 5n)	40.39
			626.63	17.80		
^{96}Tc(7$^+$)	4.28 d	ϵ(100)	778.22	99.76	^{89}Y(^{11}B, p3n)	27.78
			812.54	82.00	^{89}Y(^{11}B, d2n)	25.28
			849.86	98.00	^{89}Y(^{11}B, tn)	18.25
^{95}Tc(9/2$^+$)	20.0 h	ϵ(100)	765.79	93.80	^{89}Y(^{11}B, p4n)	36.63
					^{89}Y(^{11}B, d3n)	34.13
					^{89}Y(^{11}B, t2n)	27.10
^{94}Tc(7$^+$)	4.88 h	ϵ(100)	702.62	99.60	^{89}Y(^{11}B, p5n)	47.80
			871.09	99.99	^{89}Y(^{11}B, d4n)	45.30
					^{89}Y(^{11}B, t3n)	38.26
^{93m}Mo(21/2$^+$)	6.85 h	IT[b] (99.88)	263.06	56.7	^{89}Y(^{11}B, α3n)	21.21
			684.67	99.7	^{89}Y(^{11}B, 2p5n)	53.01
^{90m}Y(7$^+$)	3.19 h	IT(100)	202.51	97.30	^{89}Y(^{11}B, 5p5n)	77.94
			479.17	90.74	^{89}Y(^{11}B, α3p3n)	46.14
					^{89}Y(^{11}B, 2αpn)	14.34
^{101}Pd(5/2$^+$)	8.47 h	ϵ(100)	296.29	19.00	^{93}Nb(^{11}B, 3n)	19.38
			590.44	12.06		
^{100}Pd(0$^+$)	3.63 d	ϵ(100)	84.02	52.00	^{93}Nb(^{11}B, 4n)	28.64
			126.05	7.80		
^{99}Pd(5/2$^+$)	21.4 min	ϵ(100)	136.01	73.00	^{93}Nb(^{11}B, 5n)	41.07
			263.60	15.2		
^{101m}Rh(9/2$^+$)	4.34 d	ϵ(92.80),IT(7.20)	306.86	84.00	^{93}Nb(^{11}B, p2n)	16.29
					^{93}Nb(^{11}B, d2n)	13.80
					^{93}Nb(^{11}B, t)	6.80
^{100}Rh(1$^-$)	20.8 h	ϵ(100)	539.60	80.60	^{93}Nb(^{11}B, p3n)	27.36
			822.65	21.09	^{93}Nb(^{11}B, d2n)	24.87
			822.65	21.09	^{93}Nb(^{11}B, tn)	17.87
^{99m}Rh(9/2$^+$)	4.7 h	ϵ($\geqslant$99.84)	340.71	70.00	^{93}Nb(^{11}B, p4n)	36.40
			617.80	12.00	^{93}Nb(^{11}B, d3n)	33.91
					^{93}Nb(^{11}B,t2n)	26.91
^{97}Ru(5/2$^+$)	2.83 d	ϵ(100)	215.70	85.62	^{93}Nb(^{11}B, 2p5n)	52.97
			324.49	10.79	^{93}Nb(^{11}B, α3n)	21.32

[a] E_{th} denotes threshold energy.
[b] IT denotes isomeric transition.

stage of de-excitation of an excited compound nucleus. The compound nucleus cross section has the form

$$\sigma_{\alpha\beta}^{\mathrm{HF}}(E_\alpha) = \sum_{J,\Pi}\left[\pi \lambda\!\!\!^{-}{}^2 \frac{2J+1}{(2s+1)(2I+1)} \sum_{j,l} T_{\alpha jl}(E_\alpha, J, \Pi)\right] \times \left[\frac{\sum_{j',l'} T_{\beta j'l'}(E_\beta, J, \Pi)}{\sum_{\gamma, j'', l''} T_{\gamma j'' l''}(E_\gamma, J, \Pi)}\right], \quad (1)$$

where $\lambda\!\!\!^{-}$ $(= \lambda/2\pi)$ is the wavelength of incident projectile; s, I, and J represent projectile, target, and compound nucleus spin, respectively, and l is the orbital angular momentum of the projectile. $T_{\alpha jl}(E_\alpha, J, \Pi)$ stands for the transmission coefficient having channel energy E_α and orbital angular momentum l, which together with particle spin s couples to the channel angular momentum j used to select the target nucleus spin I populated for a given compound nucleus spin J and parity Π. Similarly, $T_{\beta j'l'}(E_\beta, J, \Pi)$ and $T_{\gamma j''l''}(E_\gamma, J, \Pi)$ indicate transmission coefficients for β and γ channels with emitting energies E_β, E_γ and orbital angular momenta l', l'' couple with emitting particle spins gives channel spins j', j'', respectively. The quantity in the first square bracket indicates the compound nucleus formation/fusion cross section in a state of total spin (J) and parity (Π) associated to the incident channel α which reduces to a simple form for spin less target ($I = 0$),

$$\sigma_f = \pi \lambda\!\!\!^{-}{}^2 \sum_l (2l+1) T_l. \quad (2)$$

The quantity in the second square bracket represents the decay probability of the compound nucleus in the channel β having ejectile particle energy E_β.

PACE4 uses the Bass model potential [50] for the calculation of the transmission coefficient, although it is not well suited near or below the barrier as well as for very heavy ion projectiles. Fission is considered as a decay mode, and the modified rotating liquid drop fission barrier (by Sierk [51]) is selected. The evaporation of seven light particles/nuclei in the order n, p, α, d, t, ^{3}He, ^{6}Li is considered whose transmission coefficients are determined by the optical model potential, where the optical model parameter is taken from Ref. [52]. Gilbert-Cameron (GC) nuclear level density parameter and the GC spin cutoff parameter are adopted for the calculation. Little a ratio, a_f/a_γ, is taken as unity. In order to simulate γ-multiplicity and corresponding energy, a nonstatistical yrast cascade γ-decay chain is artificially included.

2. EMPIRE3.2

EMPIRE considers all three major nuclear reaction formalisms—direct (DIR), pre-equilibrium (PEQ), and compound (EQ). DIR processes are estimated either by the coupled channels approach or distorted wave Born approximation (DWBA) [53,54]. There are various PEQ phenomenological and quantum models for light-ion induced reactions. However, PEQ emissions in the heavy-ion induced reactions are not well tested for phenomenological hybrid Monte Carlo simulation as well as quantum mechanical multistep direct (MSD) and multistep compound (MSC) models, and therefore ignored by the code. PEQ emission for heavy ion projectiles is calculated using the exciton model, which has the capability to treat the cluster emission built on the Iwamotto-Harada model [55]. The differential cross section of the PEQ emission has a form

$$\frac{d\sigma_{\alpha,\beta}}{d\epsilon_\beta} = \sigma^{\rm CF}(\epsilon_\alpha)\sum_n W_\beta(E,n,\epsilon_\beta)\tau(n), \tag{3}$$

where $\sigma^{\rm CF}(\epsilon_\alpha)$ is the composite nucleus formation cross section and defined as $\sigma^{\rm CF}(\epsilon_\alpha) = \sigma_{\rm reac}(\epsilon_\alpha) - \sigma_{\rm dir}(\epsilon_\alpha)$, a difference of reaction and direct reaction cross section. $\tau(n)$ is life-time of n exciton configuration. $W_\beta(E,n,\epsilon_\beta)$ represents the emission rate of a cluster β with energy ϵ_β, spin s_β, and reduced mass μ_β from a state with $n\ (= p + h)$ excitons and can be given as

$$W_\beta(E,n,\epsilon_\beta) = \frac{2s_\beta + 1}{\pi^2\hbar^3}\mu_\beta\epsilon_\beta\sigma_\beta^{\rm inv}(\epsilon_\beta)\left[\frac{\sum_\beta F_{lm}^\beta(\epsilon_\beta)Q_\beta^{lm}(p,h)\omega_{\rm res}(p-l,h,E-\epsilon_\beta-B_\beta)}{\omega_{\rm CN}(p,h,E)}\right], \tag{4}$$

where $\sigma_\beta^{\rm inv}(\epsilon_\beta)$ is the inverse reaction cross section; $\omega(p,h,E)$ is particle-hole state density, calculated by the Williams formula [56]. $Q_\beta^{lm}(p,h)$ is a factor accounting for the probability of the outgoing cluster β being formed with l particles situated above and m below the Fermi surface ($\beta = l + m$) and factor $F_{lm}^\beta(\epsilon_\beta)$ denotes formation probability of the cluster β as a function of its energy.

EQ processes are calculated from the Hauser-Feshbach model, including width fluctuations and the optical model for fission. However, heavy ion fusion cross section is estimated with the help of a simplified coupled channel model (CCFUS) [57]. In CCFUS, collision between two nuclei is considered in the presence of coupling of the relative motion $\vec{r}$ of the projectile to a nuclear collective motion ζ. The Hamiltonian of such a system is written as [58]

$$H(r,\zeta) = -\frac{\hbar^2\nabla^2}{2\mu} + V(r) + H^0(\zeta) + H'(r,\zeta), \tag{5}$$

where μ is the reduced mass of the system and $V(r)$ is the sum of Coulomb and nuclear Woods-Saxon potential. $H^0(\zeta)$ and $H'(r,\zeta)$ stand for the intrinsic and coupling Hamiltonian, respectively. The coupled-channels equations for the radial part of the total wave function can be written from such a Hamiltonian as

$$\left(-\frac{\hbar^2}{2\mu}\frac{d^2}{dr^2} + \frac{J(J+1)\hbar^2}{2\mu r^2} + V(r) - E + \epsilon_n\right)u_n^J(r) = -\sum_{n'} H'_{nn'}(r)u_{n'}^J(r), \tag{6}$$

where n represents a nth quantum state and ϵ_n is the energy eigenvalue of the intrinsic Hamiltonian. J is the total angular momentum, the sum of relative orbital angular momentum l, and the angular momentum of intrinsic motion I. $H'_{nn'} = \langle n|H'|n'\rangle$ is the coupling matrix element. Diagonalizing this matrix element at the barrier, the matching wave functions can be uncoupled roughly. The total transmission probability is obtained by summing over the distribution of transmission probabilities for the eigenbarriers, with weight given by the overlap of the initial state with eigenchannels,

$$T_J(E) = \sum_I \left|P_{II'}^J(E)\right|^2, \tag{7}$$

where I' is the angular momentum of collective motion in the entrance channel. Thus the fusion cross section can be calculated by using Eq. (2) except that the transmission probability is now affected by each reaction channel.

In the present calculation, the value of the mean free path parameter for the exciton model is chosen as 1.5 and the equilibrium exciton number varies between 10–14 for 25–65 MeV energy range of the projectile. The complete fusion cross section is calculated up to 21–46 $l_{\rm max}$ value for 25–65 MeV energy range using Christensen-Winther potential [59]. Various nuclear level density options, Gilbert-Cameron (GC) level density with Ignatyuk systematic, generalized superfluid model (GSM), and enhanced generalized superfluid model (EGSM), have been used.

In all three level density models, the Ignatyuk level density parameter, which consists of two independent parameters [asymptotic value of the level density parameter ($\tilde{a}$) and shell effect damping parameter (γ_s)] is used. In the GC model, the Ignatyuk systematic is used in which $\tilde{a} = 0.154A + 6.3 \times 10^{-5}A^2$ and $\gamma_s = -0.054$. GSM and EGSM use $\tilde{a} = \alpha A + \beta A^{2/3}$ and $\gamma_s = \gamma_0 A^{1/3}$, where $\alpha = 0.103$, $\beta = -0.105$, $\gamma_0 = 0.375$ are used for GSM and $\alpha = 0.0748$, $\beta = 0.0$, $\gamma_0 = 0.5609$ are used for EGSM.

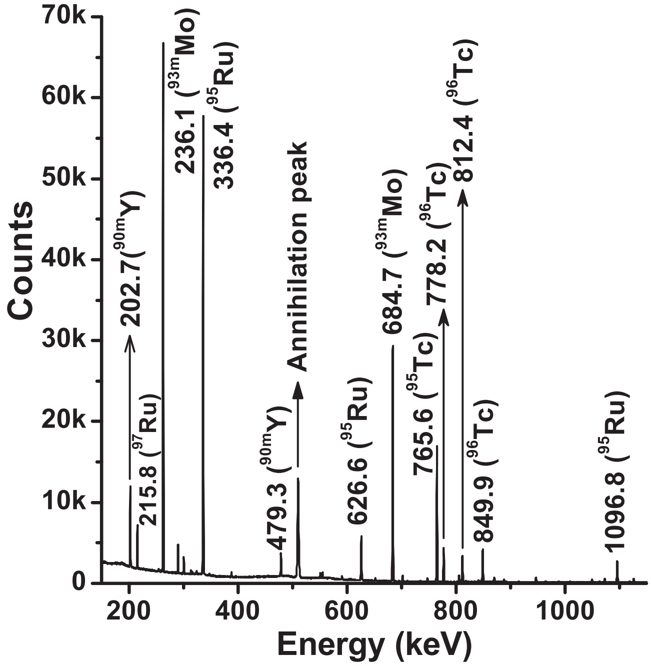

FIG. 2. A γ-ray spectrum of the ^{11}B+^{89}Y reaction at 50.8 MeV energy after 38.3 min of EOB.

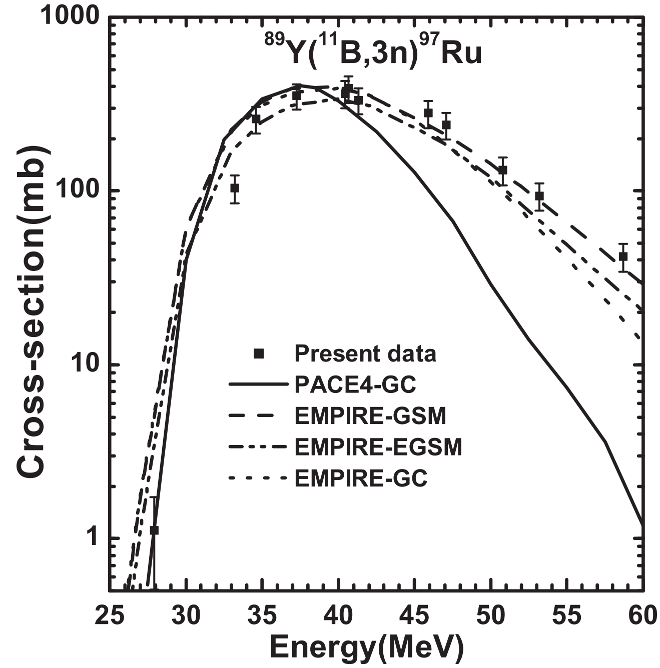

FIG. 4. Comparison of measured excitation function (symbols) of ^{97}Ru from the ^{11}B+^{89}Y reaction and those computed from the theory (curves) using EMPIRE and PACE4.

IV. RESULTS AND DISCUSSION

A methodical investigation of radioisotopes produced in the ^{11}B-induced reaction on ^{89}Y and ^{93}Nb targets was carried out for each target foil at various incident energies. Two typical γ-ray spectra collected 38.3 and 37.9 min after the EOB from the ^{11}B+^{89}Y and ^{11}B+^{93}Nb reactions at 50.8 and 51 MeV incident energies are shown in Figs. 2 and 3, respectively.

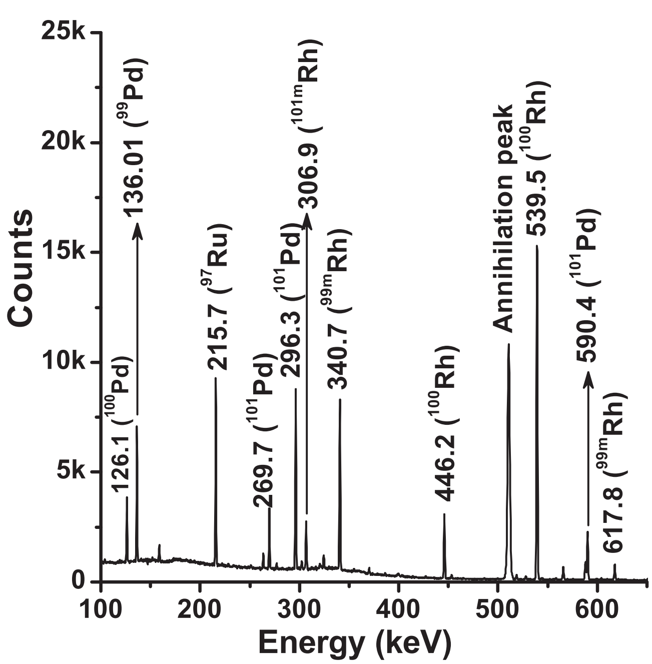

FIG. 3. A γ-ray spectrum of the ^{11}B+^{93}Nb reaction at 51 MeV energy after 37.9 min of EOB.

Production of ^{97,95}Ru, ^{96,95,94}Tc, ^{93m}Mo, ^{90m}Y residues in the ^{89}Y; and ^{101,100,99}Pd, ^{101m,100,99m}Rh, ^{97}Ru radionuclides in the ^{93}Nb target matrix are confirmed and are presented in Figs. 4–10 and Figs. 11–18, respectively. Measured data points are indicated by symbols with an uncertainty and the theoretical estimations are shown by curves.

The measured cross sections are compared with the theoretical model calculations from PACE4 and EMPIRE3.2 utilizing different nuclear level density options. A list of the radionuclides and the possible contributing reactions are listed in Table I [46]. Experimental cross section data are tabulated in Tables II and III for the ^{11}B + ^{89}Y and ^{11}B + ^{93}Nb reactions, respectively.

A. Radionuclides produced in ^{11}B+^{89}Y

1. ^{97,95}Ru

The measured excitation function of ^{97}Ru, presented in Fig. 4, is compared with the PACE and EMPIRE calculations. Experimental data are well reproduced by both the model codes in the lower energy region (∼28–42 MeV), however, the PACE estimation sharply decreases compared to the measured data at higher energies and becomes about 20 times smaller than the experimental cross section at 58.7 MeV energy. The experimental results are in good agreement with those computed from the EMPIRE at the high energy region. It certainly indicates the emission of PEQ neutrons, along with evaporated neutrons in the 3n reaction channel, as observed in various heavy-ion induced reactions [8,9,26]. Reproduction of the data describes the necessity of the PEQ exciton model used in EMPIRE for heavy projectiles. Although all the level densities show a good agreement between each other, the GSM

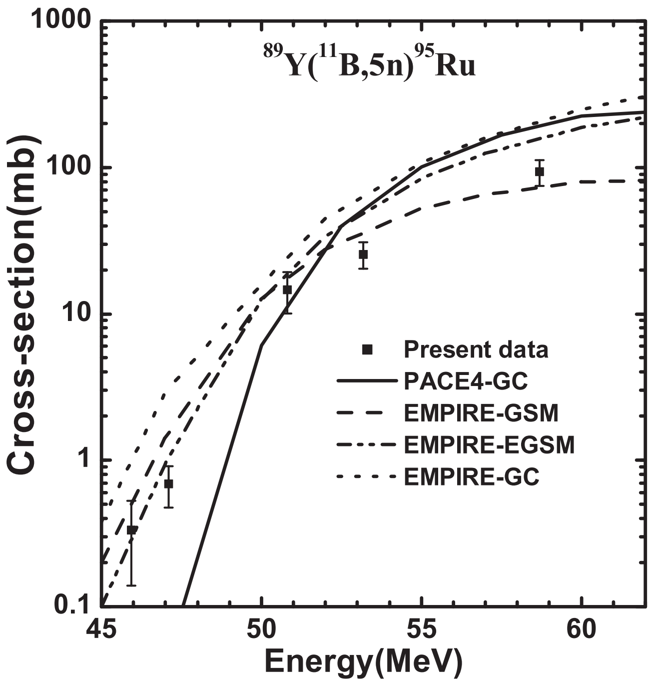

FIG. 5. Comparison of measured (symbols) and computed (curves) excitation functions for production of ^{95}Ru.

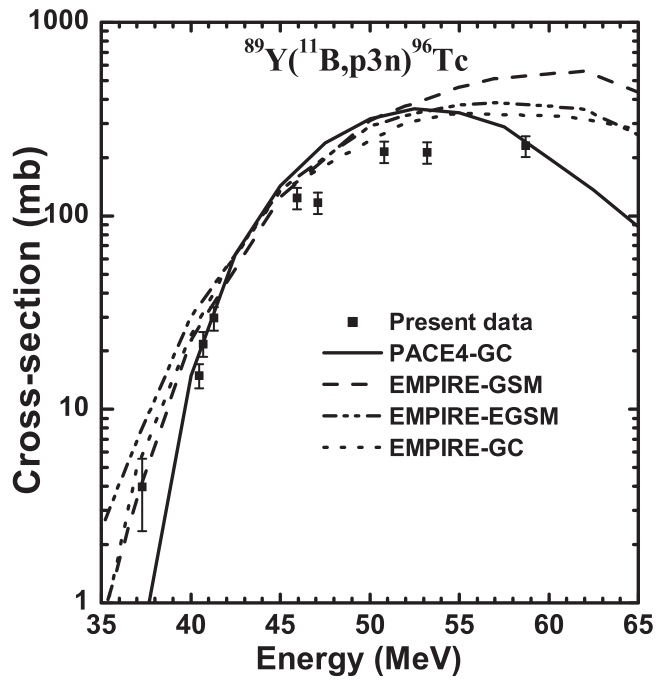

FIG. 6. Same as Fig. 5 for ^{96}Tc.

level density reproduces the measured data more accurately in comparison to the EGSM and GC level densities at the high energy tail of the excitation function.

Figure 5 shows a comparison between the measured cross sections of ^{95}Ru in the 45–60 MeV energy range and the theoretical evaluation. Experimental cross sections are best explained by EMPIRE with GSM level density throughout the energy range, while the other two calculations with EGSM and GC level density overestimate the measured data in the high energy range (∼52–60 MeV). On the other hand, the PACE result underpredicts the experimental data below 52 MeV and overpredicts above it. Independent productions of ^{97,95}Ru are measured due to the absence of any precursor.

2. ^{96,95,94}Tc

Out of the two isotopes, ^{96,96m}Tc, the ground state of the long-lived ^{96}Tc (4.28 d) was identified. Direct identification of the ^{96m}Tc (51.5 m) radionuclide is hardly possible due to its single low intense γ-ray (778.22 keV, 1.9% intensity) common with the high intensity (99.76%) 778.22 keV peak of ^{96}Tc. EMPIRE predicts the maximum 6% production of ^{96m}Tc compared to ^{96}Tc production. It is expected that activity of ^{96}Tc must increase in 5–6 h cooling time due to the decay of ^{96m}Tc (IT 98%), if produced in the target matrix, into the ^{96g}Tc radionuclide, however, no such sign was observed. Experimental and theoretical excitation functions of the ^{96}Tc is shown in Fig. 6. Both PACE4 and EMPIRE data reproduce the experimental results satisfactorily in the lower energy region, but overestimate in the high energy region.

In Fig. 7, experimental cross sections of the short-lived ^{95}Tc (20.0 h) are shown along with the theoretical excitation functions. The measured data are satisfactorily reproduced by EMPIRE and PACE4 in the higher energy region, while PACE underpredicts them in the lower energy range. The EMPIRE calculation corresponding to EGSM and GC has shown the best reproduction of measured data throughout the estimated energy range. Cumulative production of ^{95}Tc may be possible from ^{95}Ru radionuclides via the electron-capture (ϵ-decay) process. However, a trace of ^{95m}Tc was not observed in this experiment.

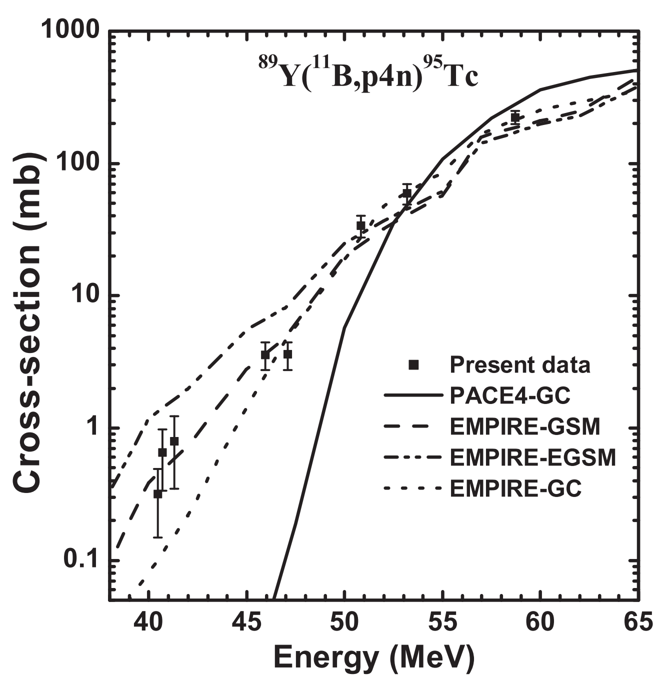

FIG. 7. Same as Fig. 5 for ^{95}Tc.

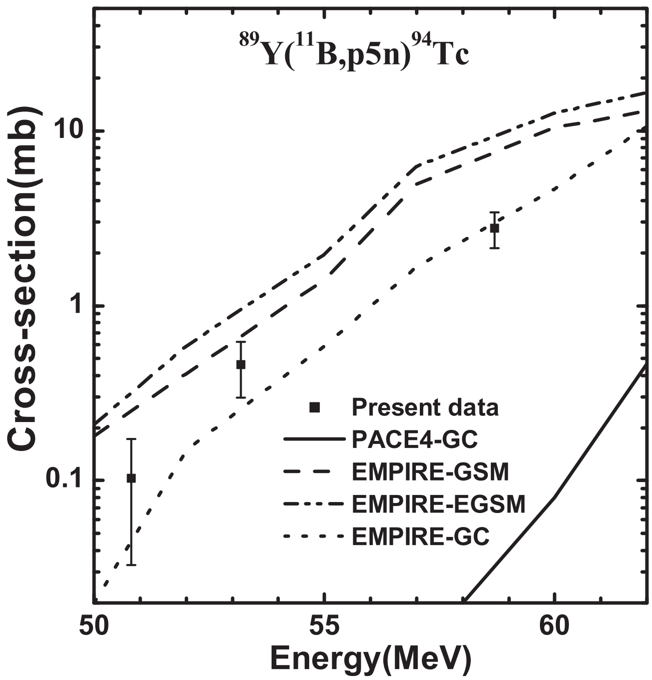

FIG. 8. Same as Fig. 5 for ^{94}Tc.

The ^{94}Tc radionuclides may be produced in both the metastable state ^{94m}Tc (52 m) and ground state ^{94}Tc (4.88 h). Due to the common γ-ray peak at 871.09 keV of ^{94m}Tc and ^{94}Tc radionuclides, it is not possible to identify ^{94m}Tc radionuclides directly. However EMPIRE predicts a significantly low isomeric ^{94m}Tc cross section compared to ^{94}Tc. The measured excitation function of ^{94}Tc, shown in Fig. 8, is well reproduced by EMPIRE with GC level density while another two level densities overestimate the measured data, particularly at the higher energy region. PACE is unable to explain the experimental observation throughout the observed energy region.

3. ^{93m}Mo

The excitation function of ^{93m}Mo is plotted in Fig. 9 to compare with the PACE and EMPIRE calculations. Experimental data are well reproduced by EMPIRE with the EGSM level density option throughout the energy range considered. Calculations of EMPIRE using other two level densities are found satisfactory below 47 MeV projectile energy and underpredict the data above it. As the code PACE calculates the cross section of ^{93}Mo, the sum of isomeric and ground state, it overpredicts the experimental data throughout (up to 55 MeV) the energy.

4. ^{90m}Y

A consistent production of ^{90m}Y radionuclide observed in the ^{11}B+^{89}Y reaction is shown in Fig. 10. The PACE4 estimation is for ^{90}Y, hence it overpredicts the EMPIRE calculation which is for ^{90m}Y. The trend of the measured excitation function is similar to those obtained from the theoretical cross sections, however, theoretical estimation is almost 10 times lower than the experimental results. Perhaps production of ^{90m}Y is an indication towards the neutron transfer from the projectile to the yttrium target.

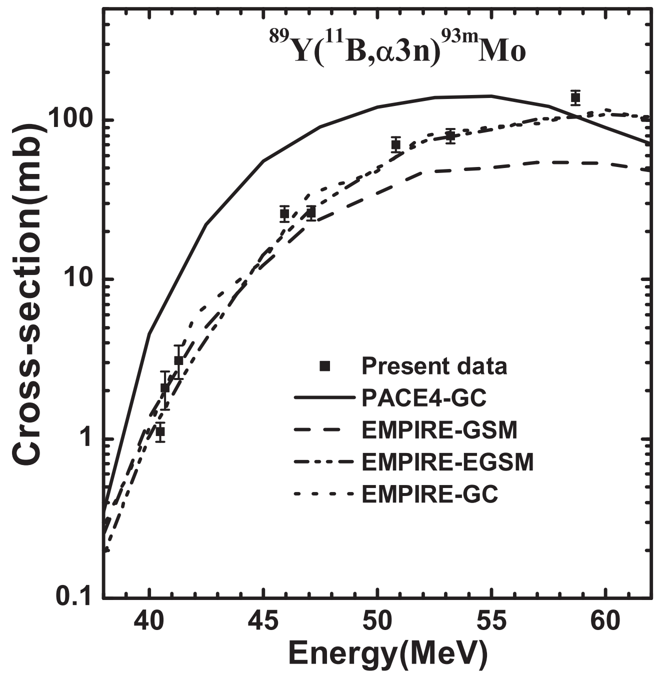

FIG. 9. Same as Fig. 5 for ^{93m}Mo.

B. Radionuclides produced in ^{11}B+^{93}Nb

1. ^{101,100,99}Pd

A comparison between the measured and theoretical excitation functions of ^{101}Pd is shown in Fig. 11. It is observed that PACE satisfactory explains the measured data below 47 MeV incident energy and falls considerably beyond

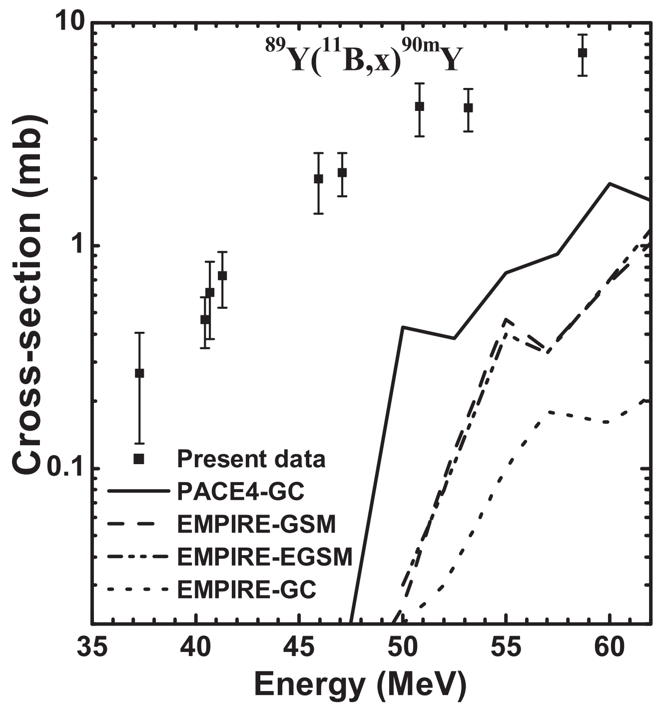

FIG. 10. Same as Fig. 5 for ^{90m}Y.

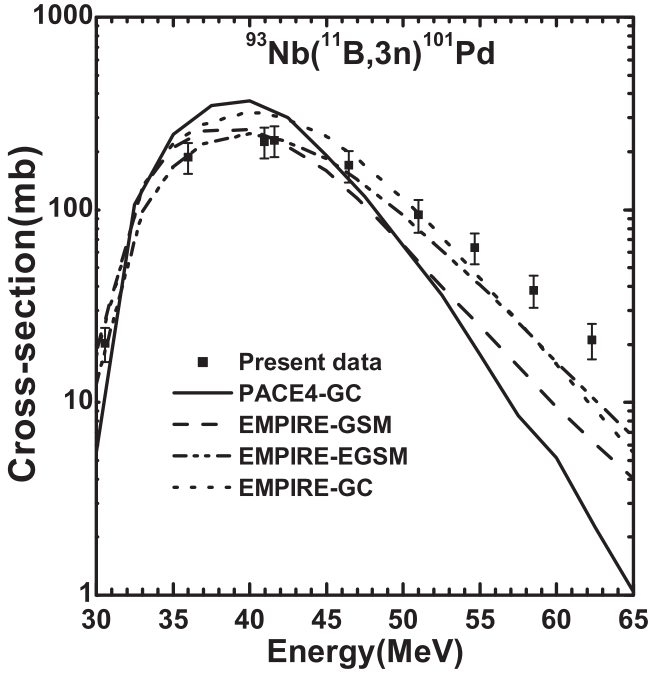

FIG. 11. Comparison of measured excitation function (symbols) of ^{101}Pd from the ^{11}B+^{93}Nb reaction and those computed from theory (curves) using EMPIRE and PACE4.

it. Overall, an experimental observation is well reproduced by EMPIRE with EGSM level density within experimental uncertainties, however a small deviation is observed above 52 MeV impinging energy. Similar to that of the 3n channel reaction in ^{11}B+^{89}Y, precompound emission of neutrons is observed over the compound reaction mechanism at the high energy tail of the excitation function. Thus direct production of ^{101}Pd is contributed by both precompound and compound nuclear processes.

Production of ^{100}Pd and ^{99}Pd at different incident energies are indicated in Figs. 12 and 13, respectively, to compare with the theoretical results. It is evident from Fig. 12 that the PACE calculation underpredicts the data at the lower energies and overpredicts at the higher energy range. Experimental data are well reproduced by the EMPIRE calculation with EGSM level density throughout the energy range within the experimental error. EMPIRE estimation with GC level density overestimates the measured data, while that with the GSM level density well reproduces up to 43 MeV energy and underestimates beyond it. On the other hand, in Fig. 13, none of the model calculation explained the experimental observations, although EMPIRE calculations mimic the trend well.

2. ^{101m,100,99m}Rh

^{101m}Rh can be produced in the target matrix either by independent reaction channels or through the decay of its precursor, ^{101}Pd. Due to the comparatively shorter half-life, ^{101}Pd (8.47 h) would decay to ^{101m}Rh (4.34 d), hence cumulative production would increase if a long cooling time is allowed. Cumulative yield of ^{101m}Rh in different half-lives of ^{101}Pd has been shown in Fig. 14 for various projectile energies.

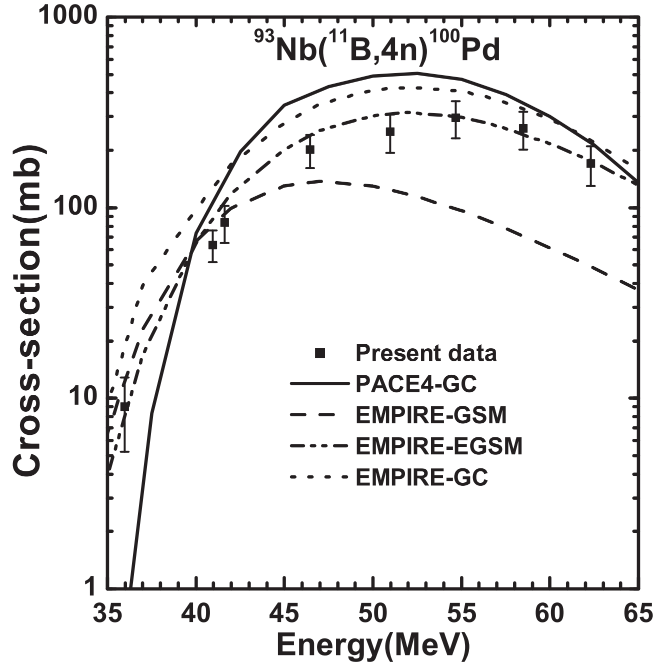

FIG. 12. Same as Fig. 11 for ^{100}Pd.

Exponential increment of the cross section through the decay of its higher charge isobar (^{101}Pd) has been observed with the passage of time, as expected. On an average, ∼55% increment in the cross section of ^{101m}Rh is observed for all the energies at the first half-life of ^{101}Pd after the EOB. However, independent production cross sections of ^{101m}Rh are measured in this work and the excitation function is shown in Fig. 15. PACE explains the data up to 51 MeV incident energy and underpredicts above it. EMPIRE calculations with EGSM and GC level density

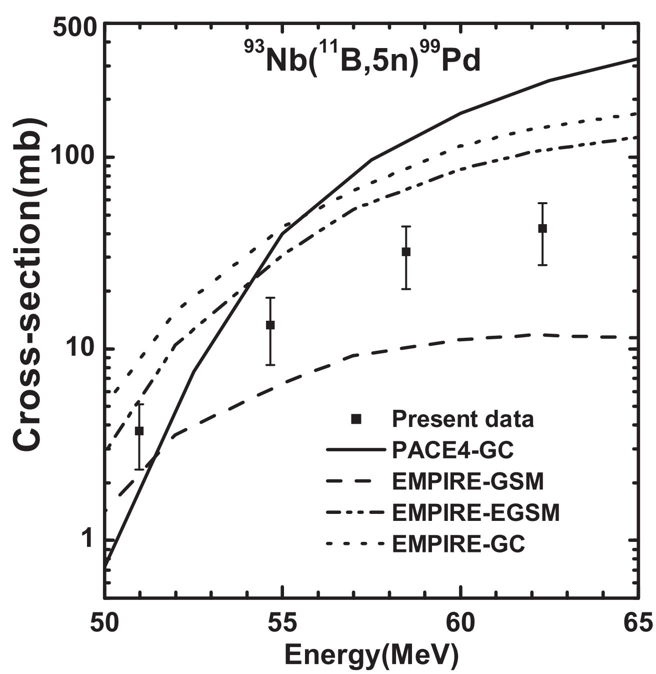

FIG. 13. Same as Fig. 11 for ^{99}Pd.

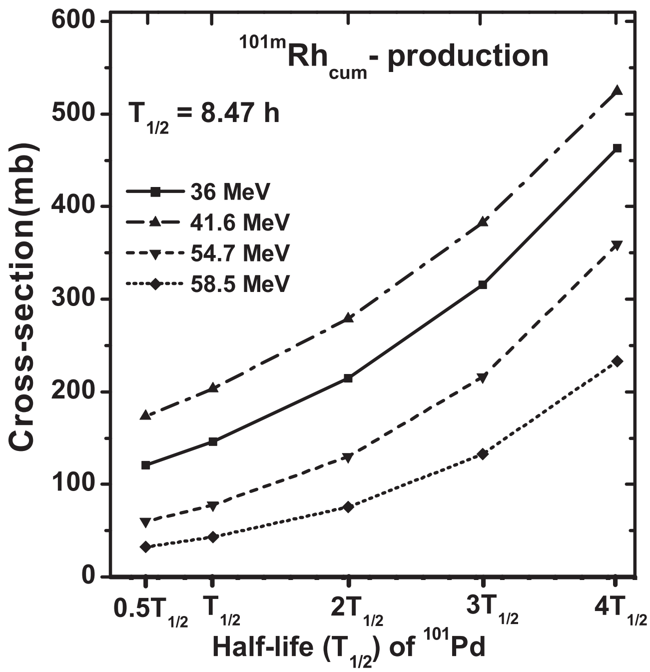

FIG. 14. Cumulative production of ^{101m}Rh, via its higher charge isobar, ^{101}Pd (8.47 h) with the passage of time at various incident energies.

reproduce the experimental data within the error bar over the energy region, while GSM overestimates beyond 40 MeV projectile energy. Nevertheless, the EMPIRE calculation shed light on the role of the PEQ reaction mechanism to ^{101m}Rh at the high energy tail.

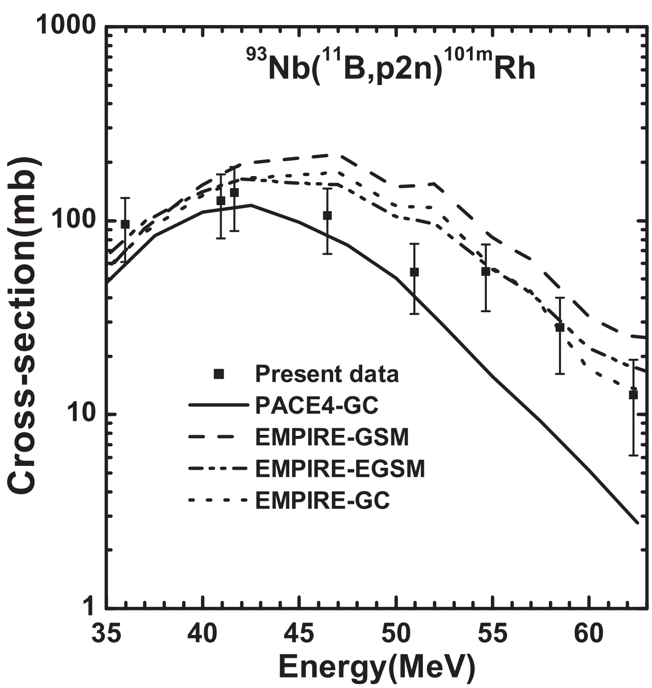

FIG. 15. Same as Fig. 11 for ^{101m}Rh.

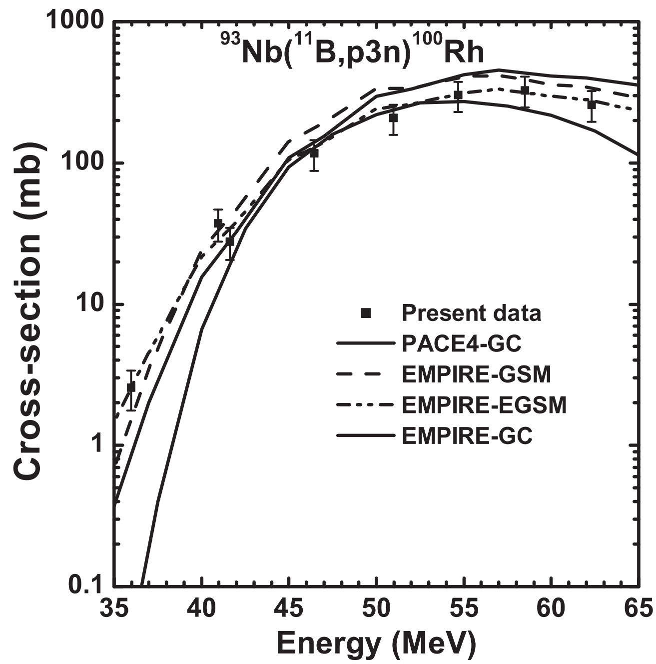

FIG. 16. Same as Fig. 11 for ^{100}Rh.

The ^{100}Rh has a metastable state ^{100m}Rh (4.6 m, IT = 98.3% and ϵ = 1.7%) and a relatively long-lived ground state ^{100}Rh (20.8 h). Metastable ^{100m}Rh could not be identified due to its short half-life. Thus a measured cross section of ^{100}Rh is the collective cross section contributed by the independent production routes and the decay from ^{100m}Rh, if it was produced. Various possible production routes of ^{100}Rh are listed in Table I. Figure 16 shows a comparison between the measured data and the calculations for ^{100}Rh. EMPIRE calculations satisfactorily predict the experimental results, while the PACE calculation shows a small deviation both in the lower and higher energy sides. EMPIRE with EGSM has best reproduced the experimental results. Although the decay of ^{100}Pd (3.63 d) could add to the cross section of ^{100}Rh, this possibility was avoided recording the γ-ray spectrum immediately after the EOB.

The metastable ^{99m}Rh (4.7 h) that mainly decays to stable ^{99}Ru ($\epsilon \geqslant$ 99.84%) was produced in the target matrix. EMPIRE calculations also support the isomeric production along with minute production of ground state ^{99}Rh. The measured excitation function of ^{99m}Rh is shown in Fig. 17 and compared the isomeric production obtained from EMPIRE along with PACE that calculates the sum of isomeric and ground state production. EMPIRE with GC explains the experimental result slightly better than EGSM and GSM level density calculations. PACE grossly underestimates the measured excitation function throughout the entire energy range.

3. ^{97}Ru

Figure 18 represents a comparison between experimental data of ^{97}Ru and the theoretical estimations. Measured results are best described by the EMPIRE with EGSM level density. The EMPIRE estimate with GC underpredicts and that with

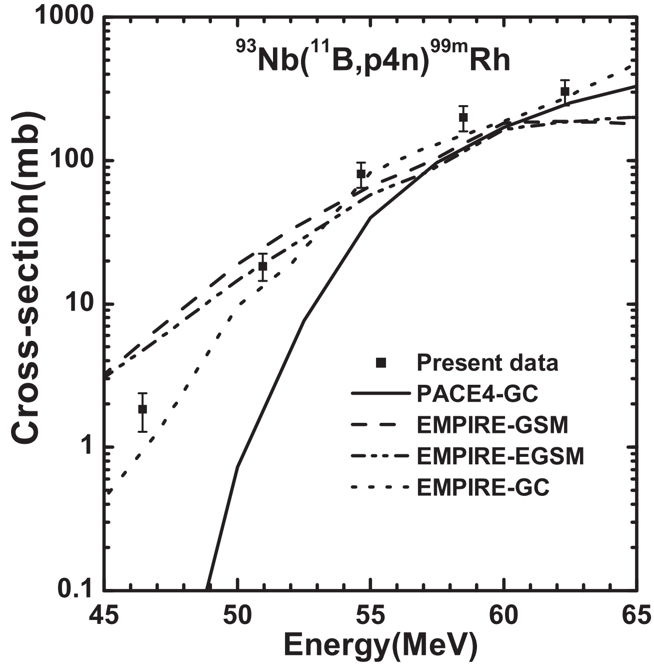

FIG. 17. Same as Fig. 11 for ^{99m}Rh.

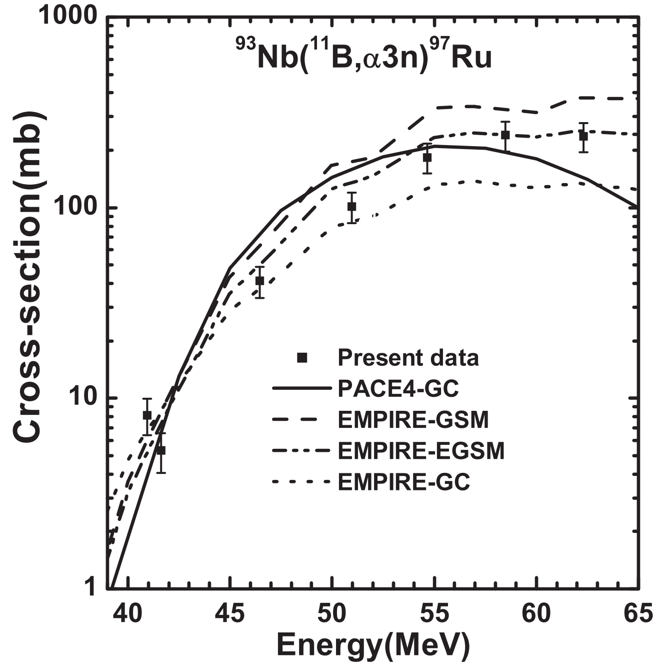

FIG. 18. Same as Fig. 11 for ^{97}Ru.

GSM overpredicts the measured excitation function above 52 MeV impinging energy. PACE data satisfactory explain the experimental observation.

In general, measured cross section data are well reproduced by EMPIRE over PACE4. In the low energy region, a gradual increase in the theoretical cross sections of the radionuclides is observed in EMPIRE calculations compared to the steep increment in PACE4. It might be due to the more accurate treatment of the fusion cross section (CCFUS) calculation and a general consideration of the Ignatyuk energy-dependent level density parameter in EMPIRE. Moreover, EMPIRE successfully explained the PEQ emission of particles in both reactions using the exciton model over the compound process. Though the effectiveness of the level density models (EGSM/GSM/GC) could not be concluded precisely from this study, yet GSM/EGSM explains satisfactorily most of the reaction channels.

C. Medically relevant radionuclides

Significant cross section (above 200 mb) of the ^{97}Ru radionuclide is observed in the 34.6–47.1 MeV wide energy spectrum in which 40.7 MeV projectile energy witnessed the maximum production cross section of ~389 mb. Production of most of the contaminants such as ^{95}Ru, ^{94}Tc, ^{93m}Mo, and ^{90m}Y are negligibly small in the desired energy range and would ultimately decay out due to their short half-lives. Therefore, only ^{97}Ru and ^{95}Tc will be abundant after a day, which can be separated chemically [28–30].

On the other hand, production of ^{101m}Rh (direct and cumulative) is possible within the 36–51 MeV energy range in

TABLE II. Cross section (mb) of radioisotopes at various incident energies in the ^{11}B + ^{89}Y reaction.

Energy (MeV)	Cross section (mb)						
	^{97}Ru	^{95}Ru	^{96}Tc	^{95}Tc	^{94}Tc	^{93m}Mo	^{90m}Y
27.9	1.1 ± 0.6						
33.2	103.6 ± 18.8						
34.6	259.6 ± 46.1						
37.3	353.4 ± 58.5		4 ± 1.6				0.3 ± 0.1
40.5	364.4 ± 64.2		14.9 ± 2.1	0.3 ± 0.2		1.1 ± 0.2	0.5 ± 0.1
40.7	389.3 ± 68.9		21.8 ± 3.2	0.6 ± 0.3		2.1 ± 0.6	0.6 ± 0.2
41.3	333.2 ± 55.7		29.6 ± 4.1	0.8 ± 0.4		3.1 ± 0.7	0.7 ± 0.2
45.9	280.1 ± 49.8	0.3 ± 0.2	123.9 ± 16	3.6 ± 0.8		25.9 ± 2.9	2 ± 0.6
47.1	239.4 ± 42.4	0.7 ± 0.2	116.8 ± 14.8	3.6 ± 0.8		26.1 ± 2.7	2.1 ± 0.5
50.8	131.7 ± 23.7	14.7 ± 4.6	214.3 ± 27.2	33.9 ± 6.2	0.2 ± 0.1	70.5 ± 7.5	4.2 ± 1.1
53.2	93.9 ± 16.8	25.5 ± 5.2	212.6 ± 26.5	59.6 ± 10.5	0.5 ± 0.2	79.6 ± 8.1	4.2 ± 0.9
58.7	41.8 ± 7.7	93.1 ± 18.7	229.8 ± 28.7	223.2 ± 25.9	2.8 ± 0.6	138.3 ± 13.9	7.3 ± 1.5

TABLE III. Cross section (mb) of radioisotopes at various incident energies in the ^{11}B + ^{93}Nb reaction.

Energy (MeV)	**Cross section (mb)**						
	^{101}Pd	^{100}Pd	^{99}Pd	^{101m}Rh	^{100}Rh	^{99m}Rh	^{97}Ru
30.6	20.3 ± 4.1						
36	187.4 ± 34	9 ± 1.9		96.1 ± 35.1	2.6 ± 0.8		
41	225.9 ± 40.8	63.9 ± 12.3		127 ± 45.9	37.2 ± 9.4		8.2 ± 1.8
41.6	229.7 ± 41.8	51.3 ± 10		139 ± 50.3	27.7 ± 7.1		5.3 ± 1.3
46.4	170.1 ± 31.5	134.5 ± 25.6		106.6 ± 39.4	116.6 ± 28.8	1.8 ± 0.6	41.3 ± 7.7
51	94.2 ± 18.3	177.5 ± 33.7	3.7 ± 1.4	54.4 ± 21.4	208.1 ± 51.1	18.4 ± 4	101.6 ± 18.5
54.7	63.9 ± 11.7	296.9 ± 65.4	13.3 ± 5.1	54.7 ± 20.6	302.8 ± 73.3	80.5 ± 16.1	183.6 ± 32.4
58.5	38.3 ± 7.4	260.5 ± 58.6	32.1 ± 11.6	28.1 ± 11.9	327 ± 79.2	199.8 ± 40.1	240.2 ± 42.5
62.3	21.1 ± 4.4	170.5 ± 40.1	42.5 ± 15.1	12.7 ± 6.5	258.4 ± 62.6	301.4 ± 59.7	236.5 ± 41.7

the ^{11}B+^{93}Nb reaction. Maximum production cross sections of ^{101m}Rh (139 mb) and its precursor ^{101}Pd (229.7 mb) that decays into ^{101m}Rh is measured in the 41.6 MeV energy. A significant quantity of ^{101m}Rh could be achieved after an appropriate cooling time.

It is true that heavy ion reactions cannot compete with the light ion production routes (of ^{97}Ru, ^{101m}Rh) in terms of the production yield. However, sufficient production of those radionuclides is possible to conduct the experiments in the laboratory scale. A good quantity of those radionuclides could be produced using a high current heavy ion accelerator. The significance of the heavy ion induced production route of ^{97}Ru and ^{101m}Rh from the target matrices Y and Nb, respectively, and their subsequent chemical separation procedures have been discussed in detail in our recent articles [30,60].

V. SUMMARY

For the first time, a detailed investigation of the excitation functions of the evaporation residues produced in the ^{11}B-induced reaction on ^{89}Y and ^{93}Nb targets was carried out and the theoretical support was provided in order to extract information about their production mechanism. It might be helpful to optimize the production parameters of medically relevant radionuclides: ^{97}Ru, ^{101m}Rh. A comparative study of the various level density models (GSM/EGSM/GC) used in EMPIRE is reported in this article. Although, no specific level density model could be suggested to explain the ^{11}B+^{89}Y and ^{11}B+^{93}Nb reaction data, EGSM/GSM calculations reproduced the measured data in many channels. In general, EMPIRE calculations show better reproduction of the cross sections in most of the channels. The comparisons of the theoretical model calculations suggest that the compound reaction mechanism is the dominant route for the production of residues. Like other heavy-ion induced reactions, PEQ emission of neutrons was observed in the $3n$ channels for both the reactions. A signature of PEQ emission was also evident in the $p2n$ and $p3n$ channel in the ^{11}B+^{93}Nb reaction. Unlike theoretical expectation, a steady and substantial production of ^{90m}Y radionuclides was observed at all energies which might be the consequence of the neutron transfer processes in the ^{11}B+^{89}Y reaction. Satisfactory reproduction of measured data by the EMPIRE calculations indicate the dependence of collective effects, considered in EGSM/GSM level density, on the compound and PEQ processes, and the effectiveness of CCFUS calculations used for heavy ion fusion cross section.

ACKNOWLEDGMENTS

The authors sincerely acknowledge the technical help and cooperation received from Professor S. Lahiri, SINP, Kolkata, during the experiment, and also thank the Pelletron staff, target laboratory staff of the BARC-TIFR Pelletron facility for their assistance during the experiment. Fellowship from MHRD, grants of IITR/SRIC/218/FIG, Government of India, are gratefully acknowledged.

[1] B. B. Back, H. Esbensen, C. L. Jiang, and K. E. Rehm, Rev. Mod. Phys. **86**, 317 (2014).
[2] L. F. Canto, P. R. S. Gomes, R. Donangelo, J. Lubian, and M. S. Hussein, Phys. Rep. **596**, 1 (2015).
[3] D. J. Parker, P. Vergani, E. Gadioli, J. J. Hogan, F. Vettore, E. Gadioli-Erba, E. Fabrici, and M. Galmarini, Phys. Rev. C **44**, 1528 (1991).
[4] G. R. Kelly, N. J. Davis, R. P. Ward, B. R. Fulton, G. Tungate, N. Keeley, K. Rusek, E. E. Bartosz, P. D. Cathers, D. D. Caussyn, T. L. Drummer, and K. W. Kemper, Phys. Rev. C **63**, 024601 (2000).
[5] M. Dasgupta, P. R. S. Gomes, D. J. Hinde, S. B. Moraes, R. M. Anjos, A. C. Berriman, R. D. Butt, N. Carlin, J. Lubian, C. R. Morton, J. O. Newton, and A. Szanto de Toledo, Phys. Rev. C **70**, 024606 (2004).
[6] D. R. Zolnowski, H. Yamada, S. E. Cala, A. C. Kahler, and T. T. Sugihara, Phys. Rev. Lett. **41**, 92 (1978).
[7] H. Timmers, D. Ackermann, S. Beghini, L. Corradi, J. H. He, G. Montagnoli, F. Scarlassara, A. M. Stefanini, and N. Rowley, Nucl. Phys. A **633**, 421 (1998).
[8] P. Vergani, E. Gadioli, E. Vaciago, E. Fabrici, E. Gadioli Erba, M. Galmarini, G. Ciavola, and C. Marchetta, Phys. Rev. C **48**, 1815 (1993).

[9] M. K. Sharma, P. P. Singh, D. P. Singh, A. Yadav, V. R. Sharma, I. Bala, R. Kumar, Unnati, B. P. Singh, and R. Prasad, Phys. Rev. C **91**, 014603 (2015).

[10] A. Shrivastava, A. Navin, N. Keeley, K. Mahata, K. Ramachandran, V. Nanal, V. V. Parkar, A. Chatterjee, and S. Kailas, Phys. Lett. B **633**, 463 (2006).

[11] D. J. Hinde, R. du Rietz, and M. Dasgupta, Eur. Phys. J. Web Conf. **17**, 04001 (2011).

[12] D. J. Hinde, R. G. Thomas, R. du Rietz, A. Diaz-Torres, M. Dasgupta, M. L. Brown, M. Evers, L. R. Gasques, R. Rafiei, and M. D. Rodriguez, Phys. Rev. Lett. **100**, 202701 (2008).

[13] G. Wallerstein *et al.*, Rev. Mod. Phys. **69**, 995 (1997).

[14] C. L. Jiang, K. E. Rehm, H. Esbensen, R. V. F. Janssens, B. B. Back, C. N. Davids, J. P. Greene, D. J. Henderson, C. J. Lister, R. C. Pardo, T. Pennington, D. Peterson, D. Seweryniak, B. Shumard, S. Sinha, X. D. Tang, I. Tanihata, S. Zhu, P. Collon, S. Kurtz, and M. Paul, Phys. Rev. C **71**, 044613 (2005).

[15] A. M. Stefanini, G. Montagnoli, R. Silvestri, S. Beghini, L. Corradi, S. Courtin, E. Fioretto, B. Guiot, F. Haas, D. Lebhertz, N. Mărginean, P. Mason, F. Scarlassara, R. N. Sagaidak, and S. Szilner, Phys. Rev. C **78**, 044607 (2008).

[16] K. E. Rehm, H. Esbensen, C. L. Jiang, B. B. Back, F. Borasi, B. Harss, R. V. F. Janssens, V. Nanal, J. Nolen, R. C. Pardo, M. Paul, P. Reiter, R. E. Segel, A. Sonzogni, J. Uusitalo, and A. H. Wuosmaa, Phys. Rev. Lett. **81**, 3341 (1998).

[17] A. M. Vinodkumar, W. Loveland, R. Yanez, M. Leonard, L. Yao, P. Bricault, M. Dombsky, P. Kunz, J. Lassen, A. C. Morton, D. Ottewell, D. Preddy, and M. Trinczek, Phys. Rev. C **87**, 044603 (2013).

[18] C. Signorini, Nucl. Phys. A **616**, 262 (1997).

[19] M. Maiti and S. Lahiri, Phys. Rev. C **79**, 024611 (2009).

[20] S. C. Srivastava, P. Som, G. Meinken, A. Sewatkar, and T. H. Ku, Brookhaven National Laboratory Report No. BNL 24614 (1978).

[21] M. C. Lagunas-Solar, M. J. Avila, N. J. Nvarro, and P. C. Johnson, Int. J. Appl. Radiat. Isot. **34**, 915 (1983).

[22] N. G. Zaitseva, E. Rurarz, M. Vobecky, K. H. Hwan, K. Nowak, T. Tethal, V. A. Khalkin, and L. M. Popinenkova, Radiochim. Acta **56**, 59 (1992).

[23] D. Comar and C. Crouzel, Radiochem. Radioanal. Lett. **27**, 307 (1976).

[24] G. Comparetto and S. M. Qaim, Radiochim. Acta **27**, 177 (1980).

[25] P. J. Pao, J. L. Zhou, D. J. Silvester, and S. L. Waters, Radiochem. Radioanal. Lett. **46**, 21 (1981).

[26] D. Kumar, M. Maiti, and S. Lahiri, Phys. Rev. C **94**, 044603 (2016).

[27] M. Maiti and S. Lahiri, Radiochim. Acta **99**, 359 (2011).

[28] M. Maiti and S. Lahiri, Radiochim. Acta **103**, 7 (2015).

[29] M. Maiti, Radiochim. Acta **101**, 437 (2013).

[30] D. Kumar, M. Maiti, and S. Lahiri, Sep. Sci. Tech. (2017), doi:10.1080/01496395.2017.1279179

[31] K. L. Scholz, V. J. Sodd, and J. W. Blue, Int. J. Appl. Radiat. Isot. **28**, 207 (1977).

[32] M. C. Lagunas-Solar, S. R. Wilkins, and D. W. Paulson, J. Radioanal. Chem. **68**, 245 (1982).

[33] M. C. Lagunas-Solar, M. J. Avila, and P. C. Johnson, Int. J. Appl. Radiat. Isot. **35**, 743 (1984).

[34] F. Ditrói, F. Tárkányi, S. Takács, I. Mahunka, J. Csikai, A. Harmanne, M. S. Uddin, M. Hagiwara, M. Baba, T. Ido, Yu. Shubin, and A. I. Dityuk, J. Radional. Nucl. Chem. **272**, 231 (2007).

[35] A. Hermanne, M. Sonck, A. Fenyvesi, and L. Daraban, Nucl. Instrum. Methods Phys. Res. B **170**, 281 (2000).

[36] S. Sudár, F. Cserpák, and S. M. Qaim, Appl. Radiat. Isot. **56**, 821 (2002).

[37] M. S. Uddin, M. Hagiwara, M. Baba, F. Tarkanyi, and F. Ditroi, Appl. Radiat. Isot. **62**, 533 (2005).

[38] A. Harmanne, M. Sonck, S. Takács, F. Tárkányi, and Yu. Shubin, Nucl. Instrum. Methods Phys. Res. B **187**, 3 (2002).

[39] F. Ditrói, F. Tárkányi, S. Takács, A. Hermanne, H. Yamazaki, M. Baba, A. Mohammadi, and A. V. Ignatyuk, Nucl. Instrum. Methods Phys. Res. B **269**, 1963 (2011).

[40] A. Hermanne, F. Tárkányi, S. Takács, and F. Ditrói, Nucl. Instrum. Methods Phys. Res. B **362**, 110 (2015).

[41] F. Ditrói, F. Tárkányi, S. Takács, A. Hermanne, A. V. Ignatyuk, and M. Baba, Nucl. Instrum. Methods Phys. Res. B **270**, 61 (2012).

[42] Ye. Skakun and S. M. Qaim, Appl. Radiat. Isot. **66**, 653 (2008).

[43] J. F. Ziegler, M. D. Ziegler, and J. P. Biersack, Nucl. Instrum. Methods Phys. Res. B **268**, 1818 (2010).

[44] M. Maiti and S. Lahiri, Phys. Rev. C **84**, 067601 (2011).

[45] M. Maiti, Phys. Rev. C **84**, 044615 (2011).

[46] http://www.nndc.bnl.gov/nudat2/ (National Nuclear Data Center, Brookhaven National Laboratory).

[47] B. Wilke and T. A. Fritz, Nucl. Instrum. Methods **138**, 331 (1976).

[48] J. Kemmer and R. Hofmann, Nucl. Instrum. Methods **176**, 543 (1980).

[49] A. Gavron, Phys. Rev. C **21**, 230 (1980).

[50] R. Bass, Phys. Rev. Lett. **39**, 265 (1977).

[51] A. J. Sierk, Phys. Rev. C **33**, 2039 (1986).

[52] C. M. Perey and F. G. Perey, At. Data Nucl. Data Tables **17**, 1 (1976).

[53] J. Raynal, Optical-Model and Coupled-Channel Calculations in Nuclear Physics, International Atomic Energy Agency Report No. IAEA-SMR-9/8 (1972).

[54] J. Raynal, *Computing as a Language of Physics*, ICTP International Seminar Course (IAEA-ICTP, Trieste, 1972), p. 281.

[55] A. Iwamoto and K. Harada, Phys. Rev. C **26**, 1821 (1982).

[56] F. C. Williams, Nucl. Phys. A **166**, 231 (1971).

[57] C. H. Dasso and S. Landowne, Comput. Phys. Commun. **46**, 187 (1987).

[58] K. Hagino and N. Takigawa, Prog. Theor. Phys. **128**, 1061 (2012).

[59] P. R. Christensen and A. Winther, Phys. Lett. B **65**, 19 (1976).

[60] D. Kumar, M. Maiti, and S. Lahiri, J. Radional. Nucl. Chem. (2017), doi:10.1007/s10967-017-5286-y.